

# Effects of differential diffusion on ignition of stoichiometric hydrogen-air by moving hot spheres

J. Melguizo-Gavilanes, R. Mével, S. Coronel, J.E. Shepherd

*Graduate Aerospace Laboratories, California Institute of Technology, Pasadena, CA 91125, USA*

---

## Corresponding Author

J. Melguizo-Gavilanes

California Institute of Technology

1200 E. California Blvd. MC 105-50

Pasadena, CA 91125 USA

E-mail: josuemg@caltech.edu

## Colloquium

Laminar Flames (Ignition)

## Word count

Method: 2

Full pages: 5 pages x 900 words/page = 4500 words

Partial pages: 1 page - 83 mm x 4.4 words/mm = 365 words

1 page - 335 mm x 2.2 words/mm = 737 words

**TOTAL length of paper: 5602 words**

---

## **Abstract**

Studying thermal ignition mechanisms is a key step for evaluating many ignition hazards. In the present work, two-dimensional simulations with detailed chemistry are used to study the effect of differential diffusion on the prediction of ignition thresholds of a stoichiometric hydrogen-air mixture by moving hot spheres. Numerical experiments showed an increase of 40 K in the minimum ignition temperature required for ignition when diffusion of species at different rates is taken into account. Detailed analysis of the species profiles at the ignition location and a sensitivity study of the system to the diffusivity of H<sub>2</sub> and H revealed the key role played by the diffusion of H atoms in preventing ignition to take place at temperatures below 1000 K.

*Keywords:* hot surface ignition, differential diffusion, minimum ignition temperature, hydrogen-air detailed chemistry

---

## **1. Introduction**

Improved scientific understanding and characterization of ignition is of prime importance for evaluating the risk of accidental fire and explosions in commercial aviation, nuclear power plants and the chemical process sector [1]. Typical thermal ignition sources include concentrated hot surfaces, moving hot particles and extended hot surfaces [2]. Common sources of heated particles are mechanical sparks in manufacturing processes and mining operations, and as a result of lightning strikes on aircraft. Previous experiments on hot particle ignition include particles heated in a furnace and then injected into explosive atmospheres [3, 4, 5], as well as stationary particles placed in flammable mixtures and heated via laser light [6, 7, 8, 9, 10, 11]. This work focuses on the former configuration. Silver [3] found an experimental threshold of 1073 K and 1083 K for a 20% hydrogen-air mixture when using 4 and 5 mm diameter particles moving at 4 m/s, respectively. Paterson [5] used a leaner mixture (10% hydrogen-air), smaller (2 mm) and slower (1.2 m/s) particles, and found a minimum ignition temperature of 1073 K. No ignition events were reported for temperatures below 1000 K for all particle sizes and concentrations considered in [3, 5]. Previous numerical and theoretical studies have been limited to 1-D simulations of stationary particles assuming spherical symmetry [6, 7], and to stagnation point ignition of premixed combustible mixtures using boundary layer equations, one-step irreversible reactions and asymptotic approximations [12, 13, 14, 15]. The aim of this study is to understand the effects of differential diffusion on the numerical prediction of the ignition threshold of stoichiometric hydrogen-air mixtures using 2-D numerical simulations with detailed chemistry.

## 2. Computational methodology

### 2.1. Governing equations

The motion, transport and chemical reaction in the gas surrounding the particle are modeled using the variable-density reactive Navier-Stokes equations with temperature-dependent transport properties [16].

$$\partial_t(\rho) + \nabla \cdot (\rho \mathbf{u}) = 0 \quad (1)$$

$$\partial_t(\rho \mathbf{u}) + \nabla \cdot (\rho \mathbf{u} \mathbf{u}) = -\nabla p + \nabla \cdot \tau + \rho \mathbf{g} \quad (2)$$

$$\partial_t(\rho Y_i) + \nabla \cdot (\rho \mathbf{u} Y_i) = -\nabla \cdot \mathbf{j}_i + \dot{\omega}_i \quad (3)$$

$$\partial_t(\rho h_s) + \nabla \cdot (\rho \mathbf{u} h_s) = -\nabla \cdot \mathbf{j}_q + \dot{q}_{\text{chem}} \quad (4)$$

$$p = \rho \bar{R} T, \quad \tau = \mu [\nabla \mathbf{u} + (\nabla \mathbf{u})^T] - \frac{2}{3} \mu (\nabla \cdot \mathbf{u}) \mathbf{I} \quad (5)$$

In equations (1)-(5),  $\rho$ ,  $p$  and  $T$  are the gas density, pressure and temperature,  $\mathbf{u}$  is the velocity vector,  $h_s$  is the mixture sensible enthalpy,  $\mathbf{g}$  is the gravitational acceleration,  $Y_i$  is the mass fraction of species,  $\mathbf{j}_i$  is the species diffusion flux,  $\dot{\omega}_i$  represents the rate of production/consumption of species,  $\mathbf{j}_q$  is the heat flux,  $\dot{q}_{\text{chem}} = \sum_{i=1}^N \Delta h_{f,i}^o \dot{\omega}_i$  is the rate of conversion of chemical into thermal energy,  $\Delta h_{f,i}^o$  is the enthalpy of formation of species,  $\bar{R}$  is the specific gas constant,  $\tau$  is the deviatoric stress tensor,  $\mu$  is the mixture viscosity, and  $\mathbf{I}$  is the identity matrix. Radiation is neglected in the current model. The species diffusion term,  $\mathbf{j}_i$ , uses Fick's law for binary mixtures. For multicomponent mixtures where one component is present in large amounts (i.e. N<sub>2</sub> for combustion in air) all other species may be treated as trace species. Writing the binary diffusion coefficient with respect to N<sub>2</sub> only yields:

$$\mathbf{j}_i = -\rho D_i \nabla Y_i, \quad \text{with } D_i = D_{j,N_2} \quad (6)$$

where  $D_i$  is the effective diffusion coefficient. In Eq. 6, thermodiffusion or Soret effect has been neglected. While thermodiffusion is known to be important in hydrogen combustion systems, the purpose of this study is to quantify and assess the importance of differential diffusion on hot particle ignition. Assessing the effect of thermodiffusion will be a topic of future study.

We solve the mass conservation equation, Eq. 1, and only for  $N - 1$  species equations. The last species mass fraction, N<sub>2</sub>, is obtained by writing  $Y_{N_2} = 1 - \sum_{i=1}^{N-1} Y_i$  and absorbs all inconsistencies introduced by Fick's law. This error is negligible when the last species  $Y_{N_2}$  is in a high concentration as is the case for combustion in air [16]. The heat flux  $\mathbf{j}_q$  includes the effect of sensible enthalpy transport by diffusion

$$\mathbf{j}_q = -\frac{\kappa}{c_p} \nabla h_s + \sum_{i=1}^{N-1} h_{s,i} \left( \mathbf{j}_i + \frac{\kappa}{c_p} \nabla Y_i \right) \quad (7)$$

where  $\kappa$  and  $c_p$  are the thermal conductivity and specific heat respectively. In Eq. 7, the Dufour effect (i.e. energy flux due to a concentration gradient) has not been taken into account [17]. Substituting Eq. 6 into 7 yields:

$$\mathbf{j}_q = -\frac{\kappa}{c_p} \nabla h_s + \sum_{i=1}^{N-1} h_{s,i} \left(1 - \frac{1}{Le_i}\right) \frac{\kappa}{c_p} \nabla Y_i \quad (8)$$

where  $Le_i = \kappa/(c_p \rho D_i)$  is the Lewis number of species  $i$ . The second term on the right hand side of Eq. 8 vanishes if the Lewis numbers of all species are assumed to be unity. This approximation is common in combustion codes and is not justified in many applications [16].

The equations above are integrated in two dimensions using the Open source Field Operation And Manipulation (OpenFOAM) toolbox [18]. The spatial discretization of the solution domain is performed using finite volumes. Specifically, the convective terms were discretized using a second order, bounded TVD scheme; the mass fractions were discretized using a linear centered scheme for scalars bounded between zero and one. The diffusion terms were discretized using the linear centered scheme together with a second order, conservative scheme for the evaluation of the surface normal gradients. The linear systems that result from the discretization of the governing equations are solved through iterative techniques [19]. The PBiCG (Preconditioned Biconjugate Gradient) method is used for all linear systems including the chemical source terms preconditioned through the DILU (Diagonal Incomplete-LU) technique, whereas the Poisson equation for pressure is solved using the PCG (Preconditioned Conjugate Gradient) preconditioned by the DIC (Diagonal Incomplete Cholesky). The pressure-velocity coupling is achieved using the PIMPLE (PISO+SIMPLE) algorithm [21]. Finally, the time-step is dynamically adapted during the course of the computation based on a specified Courant number to ensure stability of the numerical scheme [20]. In the current study the Courant number used is 0.2.

## 2.2. Chemical and transport models

The chemistry is modeled using Mével's detailed mechanism for hydrogen oxidation which includes 9 species and 21 reactions [22]. The Sutherland Law [23], Eucken relation [24] and JANAF polynomials [25] are used to account for the functional temperature dependence of mixture viscosity ( $\mu$ ), thermal conductivity ( $\kappa$ ) and specific heat ( $c_p$ ) respectively. Species diffusivities are computed using Cantera [26]; a constant non-unity Lewis number,  $Le_i$ , is specified for each species. This is a convenient approximation since  $Le_i$  values are essentially constant and usually vary in small amounts across flame fronts [16]. For convenience the subscript  $i$  is dropped for the rest of the discussion.

The current numerical framework, chemical and transport models have been validated in a recent hot surface ignition study performed by the authors [27].

### 3. Domain, initial and boundary conditions

The computational domain consists of a vertical rectangle with a 2-D-axisymmetric sphere located at  $(0, 0, 0)$  with diameter  $d = 4$  mm. The top, bottom and side boundaries are placed  $15d$ ,  $5d$  and  $10d$  away from the center of the sphere, respectively. A resolution of approximately 300,000 cells is used, with finer resolution near the sphere; a minimum cell size of  $60 \mu\text{m}$  ensures that the thermal/hydrodynamic boundary layers are properly resolved.

The numerical integration is divided in two parts: first, a free fall in  $\text{N}_2$  for 0.25 s (fall time measured experimentally) during which a steady axisymmetric thermal boundary layer develops. Second, contact with reactive stoichiometric hydrogen-air mixture ( $Y_{\text{H}_2} = 0.0283$ ,  $Y_{\text{O}_2} = 0.2264$ ,  $Y_{\text{N}_2} = 0.7453$ ) for 20 ms (experimental observation window) or until ignition is observed and initial stages of flame propagation take place. The initial conditions are  $p_o = 101 \text{ kPa}$ ,  $T_o = 300 \text{ K}$ ,  $\mathbf{u}_o = (0, 0, 0) \text{ m/s}$  and a constant (uniform) sphere surface temperature,  $T_{\text{sphere}}$ , providing an isothermal boundary condition for the gas. The validity of this boundary condition was assessed using a Biot number analysis [28]. The temperature drop during the simulation test time was found to be of less than 1% for the sphere surface temperatures considered here. There is no net flux of species to the wall, and the effects of surface heterogeneous reactions have been ignored. The frame of reference is attached to the sphere, hence, a time dependent inflow boundary condition is prescribed at the bottom of the computational domain to properly simulate the fall of the heated particle, as its velocity increases at a rate of  $g = 9.81 \text{ m/s}^2$ , given by  $\mathbf{u}(t) = (0, gt, 0) \text{ m/s}$ . At the top, a non-reflective/pressure transmissive boundary condition is used to simulate an outflow.

## 4. Results and Discussion

### 4.1. 2-D ignition delay times

In Fig. 1, the ignition times obtained from the 2-D simulations for different surface temperatures computed with ( $\text{Le} \neq 1$ ) and without ( $\text{Le} = 1$ ) differential diffusion effects are plotted together with constant pressure (CP) delay times. The time to ignition,  $\tau_{\text{ign}}$ , shown in Fig. 1 was defined as the time elapsed from contact with reactive mixture until the maximum temperature in the domain reached  $T_{\text{sphere}} + 150 \text{ K}$ . For the CP calculations, the time to maximum temperature gradient is reported. The ignition time from the 2-D simulation increases rapidly as the temperature of the sphere is decreased to 960 K for  $\text{Le} = 1$  (solid), and 1000 K for  $\text{Le} \neq 1$  (dashed). The vertical asymptotes (dotted) indicate the existence of a threshold, namely, the temperature below which ignition does not occur during the simulation time (20 ms). Note that the ignition threshold increases by 40 K when differential diffusion is included. Further examination of the curve also reveals the existence of a horizontal asymptote at  $\tau_{\text{ign}} = 2.1 \text{ ms}$ ; temperatures higher than 1100 K will result in ignition immediately after contact of the sphere with reactive mixture. Above 1100 K, the reaction rates are too fast for diffusive and convective

losses to counteract the chemical heat release. Overall, the ignition delay times computed for the 2-D simulation that accounts for differential diffusion are slightly longer than their unity Le counterpart, except at the ignition threshold where the delay time is marginally shorter, 15.208 ms for  $\text{Le} \neq 1$  and 16.306 ms for  $\text{Le} = 1$ . This is due to the lower temperature threshold found for  $\text{Le} = 1$ .

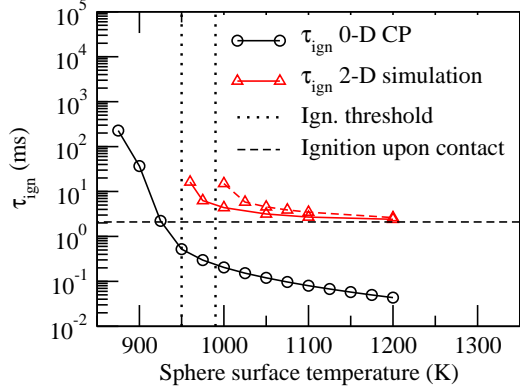


Figure 1: Comparison of ignition times obtained from 2-D simulations (unity (solid lines) and non-unity (dashed lines) Le number cases) and CP ignition delay times.

The ignition location along the sphere is characterized by the angle,  $\theta$ , measured from the vertical centerline starting at the front stagnation point ( $\theta = 0^\circ$ ) and increasing towards the rear stagnation point ( $\theta = 180^\circ$ ). The ignition location moves from the front stagnation point towards the zone of flow separation (near  $\theta = 120^\circ$ ) as the temperature decreases towards the minimum ignition temperature. For all cases considered, ignition was never observed to occur in the recirculation region, hot wake, or rear stagnation point. In contrast to the 2-D simulation ignition times, the CP ignition times continue to decrease as the initial temperature of the gas increases. The large differences observed between the two types of simulations are mostly due to differences in the initial mixture composition and the absence of convective and diffusive losses in the CP calculations. In the 2-D simulations, several milliseconds are required to create a flammable mixture in the boundary layer through diffusion (from 2 ms at the front stagnation point up to about 8 ms at the separation point (see Fig.7)), whereas the CP calculations consider a reactive mixture with fixed composition from  $t = 0$ . As chemical reactions start to take place, convective and diffusive losses counteract the formation of reactive species and subsequent thermal runaway by transporting species and heat away from the region of highest temperature in the flow field. Note also that  $\tau_{\text{ign}}$  for the 2-D simulations is plotted as a function of  $T_{\text{sphere}}$  which is typically 30 to 50 K higher than the gas temperature at the ignition location just before chemistry is activated.

#### 4.2. 2-D fields at ignition threshold

We now focus on explaining the differences observed between the simulations performed with and without Lewis number effects or differential diffusion. Of particular interest is the higher ignition threshold obtained when accounting for species diffusing at different rates. Figure 2 shows fields of  $\text{H}_2$ ,  $\text{O}_2$ , and  $\text{N}_2$ , 10 ms after

sphere contact with reactive mixture for  $\text{Le} = 1$  (left) and  $\text{Le} \neq 1$  (right). The differences become very apparent in the thickness of the interface between  $\text{H}_2$  and  $\text{N}_2$ , and the extent of  $\text{H}_2$  present in the wake. For the  $\text{Le} \neq 1$  case, concentrations of  $\text{H}_2$  greater than 0.01 reach the rear stagnation point of the sphere, however, the absence of  $\text{O}_2$  renders the mixture non-flammable and ignition is never observed to take place in this region during the experimental observation window. All these differences, as expected, are due to the high mass diffusivity of  $\text{H}_2$  into  $\text{N}_2$  compared to that of  $\text{O}_2$ .

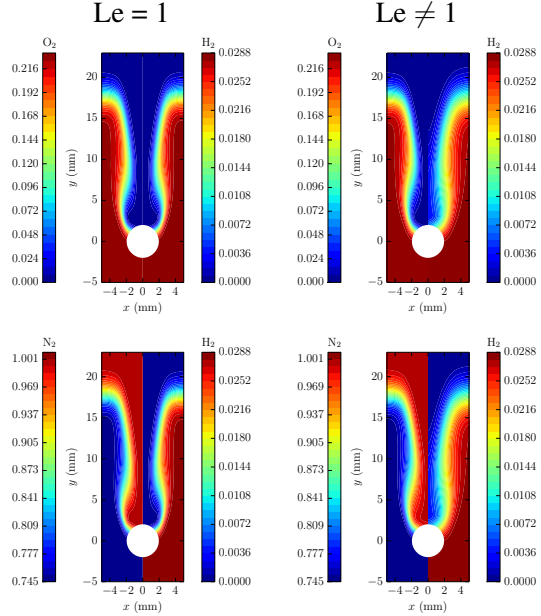


Figure 2: Comparison of mass fraction fields ( $\text{H}_2$ ,  $\text{O}_2$ , and  $\text{N}_2$ ) 10 ms after hot sphere contact with reactive mixture with ( $\text{Le} \neq 1$ ) and without ( $\text{Le} = 1$ ) differential diffusion for  $T_{\text{sphere}} = 960$  K.

Figure 3 shows velocity, temperature and mass fraction fields at the time ignition takes place for the unity  $\text{Le}$  case ( $\tau_{\text{ign}} = 16.306$  ms). An ignition kernel forms within the thermal boundary layer close to the region where flow separation occurs (see Fig. 3 top left). The mass fraction of product,  $\text{H}_2\text{O}$ , reaches 0.0573 signaling that the exothermic formation of  $\text{H}_2\text{O}$  through  $\text{OH}+\text{H}+\text{M}=\text{H}_2\text{O}+\text{M}$  and  $\text{H}_2+\text{OH}=\text{H}_2\text{O}+\text{H}$  is active, hence the gas temperature in the ignition kernel peaks to 1103 K, roughly 150 K higher than the sphere temperature. For the  $\text{Le} \neq 1$  case, no heat deposition in the gas is triggered after 16.306 ms of contact with reactive mixture, resulting in a  $\text{H}_2\text{O}$  mass fraction 7 orders of magnitude lower ( $1.24 \times 10^{-9}$ ). A less diluted wake (lower  $\text{N}_2$  concentration) is also present in this case, consistent with the higher entrainment of  $\text{H}_2$  into the boundary layer expected after allowing for 6 ms extra of diffusion.

#### 4.3. Wall heat flux and ignition location

Although the ignition location can be visually determined using the 2-D fields in Fig. 3, a more exact way of determining it is by plotting the wall heat flux along the sphere at different times during the simulation as shown in Fig. 4. The horizontal axis is normalized by  $\pi$  ( $180^\circ$ ) resulting in  $\theta/\pi = 0$  at the front stagnation point, and  $\theta/\pi = 1$  at the rear stagnation point. The horizontal black dashed line drawn at 0 wall heat flux is a visual

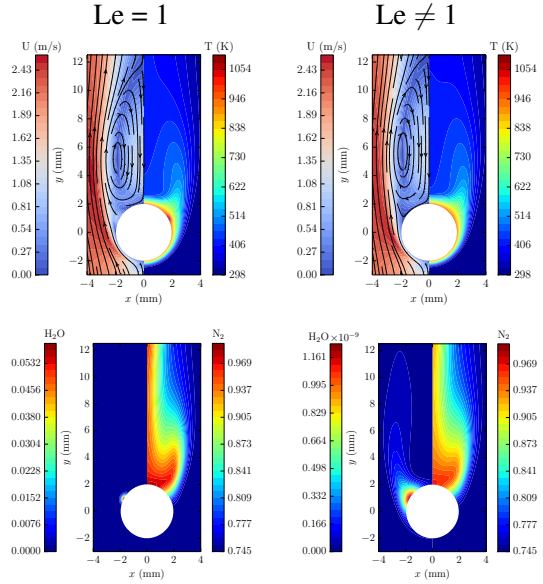


Figure 3: Comparison of temperature, velocity and mass fraction fields ( $\text{N}_2$  and  $\text{H}_2\text{O}$ ) 16.306 ms after hot sphere contact with reactive mixture with ( $\text{Le} \neq 1$ ) and without ( $\text{Le} = 1$ ) differential diffusion for  $T_{\text{sphere}} = 960 \text{ K}$ .

indicator to aid with determining the exact time and location when the heat transfer switches direction: from the sphere to the gas, positive heat flux, and from the gas to the sphere, negative heat flux, or equivalently, the onset of the exothermic step in the reaction mechanism and heat deposition in the gas. The transition takes place between  $t = 16.250$  and  $16.258$  ms, however the onset of significant chemical activity starts 0.058 ms earlier, at 16.2 ms, with the initiation step involving  $\text{H}_2$  and  $\text{O}_2$  at constant temperature and initial production of  $\text{H}$  and  $\text{O}$  atoms. Due to having a  $T_{\text{sphere}} = 960 \text{ K}$ , the low temperature non-chain branching pathways are favored, mainly those concerned with the production of  $\text{HO}_2$  (see Fig. 6). Finally, the ignition location is found at  $\theta/\pi = 0.67$  or  $\theta = 120.6^\circ$ ; this corresponds to a minimum in the wall heat flux.

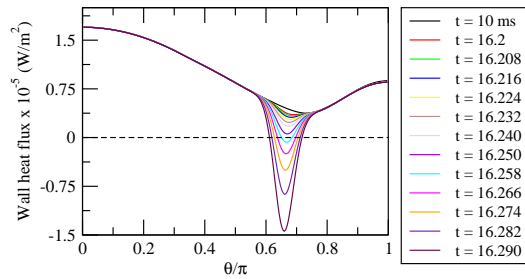


Figure 4: wall heat flux along sphere for  $T_{\text{sphere}} = 960 \text{ K}$  ( $\text{Le} = 1$ ).

#### 4.4. Energy equation analysis

Analyzing the wall heat flux along the sphere allowed us to determine the exact location where chemical activity starts and initial heat release occurs, however the ignition of the gas takes place some distance away from the surface of the sphere. Figure 5 shows the contribution of each term in the energy equation normal to the sphere surface at  $\theta = 120.6^\circ$  and  $t = 16.203$  ms. The abscissas represent the normal radial distance from the surface of the heated sphere, and the ordinates show the corresponding energy density and temperature.

The terms plotted are  $h_{\text{Convection}} = -\nabla \cdot (\rho \mathbf{u} h_s)$ ,  $h_{\text{Diffusion}} = \nabla \cdot (\kappa/c_p \nabla h_s)$ , and  $h_{\text{Source}} = \dot{q}_{\text{chem}}$ , their sum,  $h_{\text{Unsteady}}$ , and the gas temperature,  $T$ . A few important features are worth mentioning: (1) the thermal boundary layer thickness (2.5 mm) is of the same order of the radius of the sphere (2 mm); (2) the temperature maximum (ignition location) is located 0.081 mm away from the surface of the sphere; (3) close to the sphere surface, the source term is mostly balanced by diffusion but about 2 times larger at this time; (4) the dip in the convective term is due to the expansion of the gas taking place in this region as a result of the initial chemical energy release; (5) the net energy addition (sum term) is positive up to 0.5 mm away from the sphere surface. At later times, the typical structure of a flame develops as the ignition kernel grows and propagates into the surrounding reactive mixture.

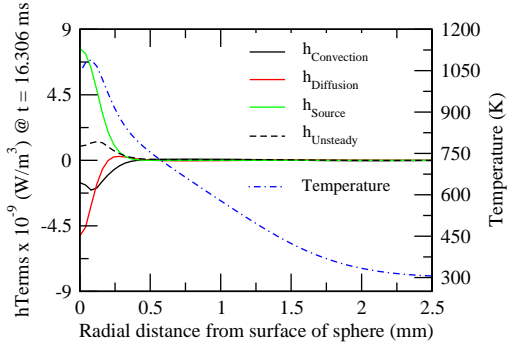


Figure 5: Contributions of each term in the energy equation and temperature normal to the surface of the sphere at  $\theta = 120.6^\circ$  for  $T_{\text{sphere}} = 960$  K ( $\text{Le} = 1$ ).

#### 4.5. Temporal evolution of species at ignition location

After finding the ignition location from the 2-D simulations ( $\theta = 120.6^\circ$ , 0.081 mm away from surface of the sphere) the temporal evolution of species for  $\text{Le} = 1$  (ignition case) and  $\text{Le} \neq 1$  (no ignition case) are monitored in detail to understand why differential diffusion pushes the ignition threshold 40 K higher. Figure 6 shows the temporal evolution of major (top) and minor (bottom) species for  $\text{Le} = 1$  at  $T_{\text{sphere}} = 960$  K during the ignition event. A sharp increase in temperature is observed along with fast consumption of the reactants,  $\text{H}_2$  and  $\text{O}_2$ , and rapid production of the combustion product,  $\text{H}_2\text{O}$ , and of very reactive transient species,  $\text{H}$ ,  $\text{O}$  and  $\text{OH}$ . The gas temperature drops after ignition indicating heat conduction from hot combustion products towards the sphere surface. The minor species profiles are characterized by a significant accumulation of  $\text{HO}_2$  radicals before ignition occurs. This indicates that as expected, under low temperature conditions, the production of  $\text{OH}$  radical is achieved through non-chain branching pathways,  $R_1: \text{H}+\text{O}_2+\text{M}=\text{HO}_2+\text{M}$  followed by  $R_2: \text{HO}_2+\text{H}=\text{OH}+\text{OH}$ , rather than through the classical chain-branching reactions:  $R_3: \text{H}+\text{O}_2=\text{O}+\text{OH}$  and  $R_4: \text{O}+\text{H}_2=\text{H}+\text{OH}$ .

To emphasize the differences between  $\text{Le} = 1$  (ignition) and  $\text{Le} \neq 1$  (no ignition) at 960 K, the species profiles at the ignition location are analyzed for both cases. Figure 7 shows the evolution of concentration of reactants from 3 ms after contact with reactive mixture to 16.3 ms (shortly before ignition takes place in the  $\text{Le} = 1$  case). The profiles show  $\text{H}_2$  diffusing rapidly into the ignition location when using the non-unity  $\text{Le}$

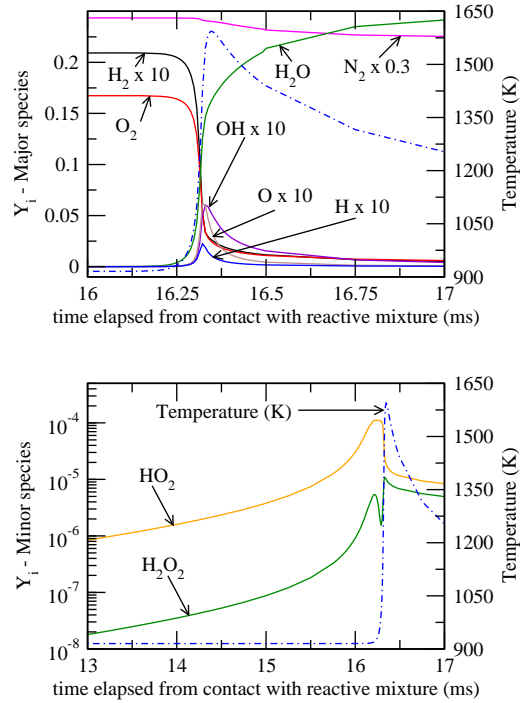


Figure 6: Temporal evolution of major and minor species and temperature at ignition location -  $\theta = 120.6^\circ$ , 0.081 mm away from surface of the sphere for  $T_{\text{sphere}} = 960$  K ( $\text{Le} = 1$ ).

formulation, resulting in an infinite equivalence ratio,  $\Phi$ , because only  $\text{H}_2$  is present at that location initially as it takes a few milliseconds longer for  $\text{O}_2$  to diffuse. The equivalence ratio slowly converges to 1.15 after 7.5 ms, indicating the presence of a slightly richer and less diluted mixture ( $\text{N}_2$  concentration is not shown in Fig. 7) when compared to the unity Le case. As expected, for  $\text{Le} = 1$ , the equivalence ratio remains constant at unity during the course of the simulation. CP calculations were performed to quantify the impact of the change of initial composition induced by differential diffusion on the ignition delay time. The composition at 15 ms after contact with the reactive mixture was selected for the computations. The delay times obtained were 9.39 ms and 9.09 ms for  $\text{Le} = 1$  and  $\text{Le} \neq 1$ , respectively. This result suggests that the increase on the ignition threshold observed for  $\text{Le} \neq 1$  is not related to the change of initial mixture composition as richer mixtures seem to ignite slightly faster.

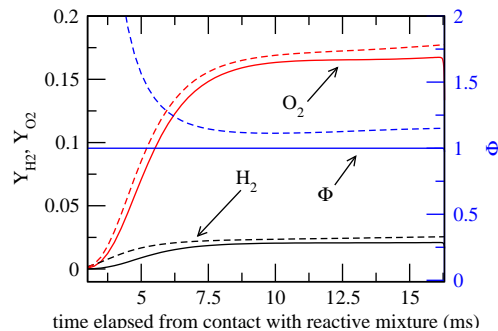


Figure 7: Temporal evolution of  $\text{H}_2$ ,  $\text{O}_2$  and equivalence ratio,  $\Phi$ , for unity (solid lines) and non-unity (dashed lines) Le cases at the ignition location -  $\theta = 120.6^\circ$ , 0.081 mm away from surface of the sphere for  $T_{\text{sphere}} = 960$  K.

The comparison of the minor species profiles, Fig. 8, clearly displays how the concentration of  $\text{H}$ ,  $\text{O}$ ,  $\text{OH}$ ,

$\text{H}_2\text{O}_2$  and  $\text{HO}_2$  achieve constant values after 5 ms when  $\text{Le} \neq 1$ . Additionally, the temperature remains essentially constant at 915 K (see Fig. 6). Conversely, in the unity Lewis number case, the concentration of all these species increases continuously and eventually induces an exponential growth of the radical pool resulting in the combined chain-branching thermal runaway characteristic of ignition events. The most likely explanation of this difference in behavior is the high mass diffusivity of H atoms. In the  $\text{Le} \neq 1$  case, the rapid diffusion of H atoms balances its production, significant build up of H cannot be achieved thereby hindering the production of OH radicals through  $R_1$  and  $R_2$ . For  $\text{Le} = 1$ , H atoms reside longer where they are produced allowing for significant build up of species and subsequent ignition at lower temperatures.

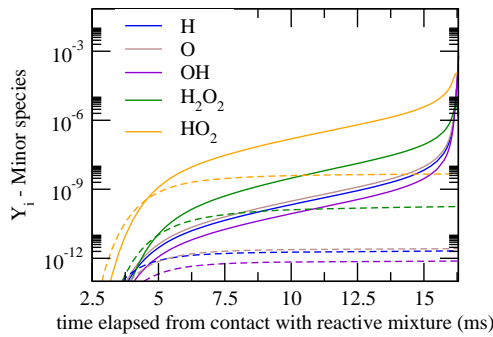


Figure 8: Temporal evolution of minor species for unity (solid lines) and non-unity (dashed lines) Le number cases at ignition location -  $\theta = 120.6^\circ$ , 0.081 mm away from surface of the sphere for  $T_{\text{sphere}} = 960$  K.

In order to test this hypothesis, additional simulations were performed to assess the effect and sensitivity of the individual species Le on the ignition threshold. First, all species Le were set to unity except for the fuel Le,  $\text{Le}_{\text{H}_2}$ , which was kept fixed at 0.28. No ignition was observed for  $T_{\text{sphere}} = 960$  K, however at 975 K the gas ignited after 7.168 ms. For  $T_{\text{sphere}} = 1000$  K, ignition took place after 4.592 ms. Both ignition times are very close to those obtained when  $\text{Le} = 1$  for all species. Second, the Le of H,  $\text{Le}_H$ , was set to 0.17 (its physical value) while keeping the Le numbers of the remaining species at unity. Ignition occurred after 12.076 ms for a sphere surface temperature of 1000 K. At 975 K and 960 K the reactive gas within the thermal boundary layer did not ignite. Allowing for H atoms to diffuse at their physical rate resulted in a higher ignition threshold. In fact, the same temperature threshold as in the non-unity Le number case (1000 K) was obtained by varying only  $\text{Le}_H$ . Regarding ignition delay times, the  $\text{Le} = 1$  with  $\text{Le}_H \neq 1$  case ignited 2.952 ms earlier than the  $\text{Le} \neq 1$  case. This outcome shows the importance of diffusion of H atoms in preventing ignition to occur at temperatures lower than 1000 K. When the Le of the intermediate species are set to unity, the H atoms do not diffuse as quickly, and accumulate close to the sphere surface allowing for enough time for their concentration to grow leading to the rapid formation of OH by  $R_2$ . On the other hand, if the proper Le number for H is used at  $T_{\text{sphere}} = 960$  K, the rate of production of H atoms is balanced by diffusion which limits the growth of  $\text{HO}_2$  and subsequently of OH radicals. The only way to counteract the loss of H atoms by diffusion is by going to higher temperatures so that a critical concentration of H is reached and the rapid production of OH is activated resulting in ignition of the

gas.

## 5. Conclusion

In the present study, the ignition of stoichiometric hydrogen-air mixtures by a moving hot sphere has been investigated. To the authors knowledge, this is the first time a 2-D simulation with detailed chemistry is performed to investigate the ignition of a combustible mixture by moving heated spheres. The purpose of the study was to quantify the effect of heat and mass transport phenomena, particularly that of differential diffusion, on the minimum ignition temperature for a given composition, sphere size and velocity. It was shown numerically that accounting for diffusion of species at different rates gave rise to an increase of 40 K (from 960 to 1000 K) in the ignition threshold. Sensitivity analyses of the system to the diffusivities of H<sub>2</sub> and H demonstrated that the loss of H atoms through diffusion was responsible for the increase in the ignition threshold. The rapid diffusion of H atoms results in a balance between chemical production and transport losses, significant build up of H cannot be achieved thereby hindering the rapid production of OH radical via HO<sub>2</sub>+H=OH+OH, and ultimately ignition. At slightly higher temperature (1000 K), the chemical production of H is sufficiently fast to overcome its diffusion losses resulting in ignition of the gas. The present results demonstrate that quantitative predictions of ignition thresholds for moving hot spheres require a detailed simulation that includes correct initial and boundary conditions, as well as adequate transport models to capture important features such as boundary layer separation, energy and species diffusion processes. Including additional physics such as surface reactions, as well as a systematic variation of the system parameters (e.g. hot surface size, mixture equivalence ratio, sphere velocity, etc.) and their effect on ignition thresholds were outside of the scope of this study and remain to be investigated in detail.

## Acknowledgements

Computing resources provided by the Extreme Science and Engineering Discovery Environment (XSEDE). JMG was supported by NSERC Postdoctoral Fellowship Program, and SC and RM by The Boeing Company through grant CT-BA-GTA-1.

## References

- [1] Guidelines for determining the probability of ignition of a released flammable mass, Center for Chemical Process Safety, AIChE 2nd Edition, Wiley, 2014, p.264.
- [2] V. Brabauskas, Ignition Handbook, Fire Science Publishers, Issaquah WA, USA, 2003, p.1116.
- [3] R.S. Silver, Phil. Mag. J. Sci., 23(156)(1937)633–657.
- [4] S. Paterson, Phil. Mag. J. Sci. 28(1939)1–23.
- [5] S. Paterson, Phil. Mag. J. Sci. 30(203)(1940)437–457.
- [6] M. Beyer, D. Markus, Sci. Technol. Energ. Ma. 79(2012)1–7.
- [7] D. Roth, P. Sharma, T. Haeber, R. Schiessl, H. Bockhorn, U. Maas, M. Beyer., D. Markus, Combust. Sci. Tech. 186(10-11)(2014)1606–1617.
- [8] T.H. Dubaniewicz, J. Laser Appl. 18(4)(2006)312–319.
- [9] H. Bothe, S. Schenk, S. Hawksworth, F.B. Carleton, F.J. Weinberg, Explosion Safety in Hazardous Areas, 1999. International Conference on (Conf. Publ. No. 469), 1999.
- [10] F. Beyrau, M.A. Hadjipanayis, R.P. Lindstedt, Proc. Comb. Inst. 34(2013)2065–2072.
- [11] H.S. Homan, Proc. Comb. Inst. 18(1981)1709–1717.
- [12] C.K. Law, Int. J. Heat Mass Tran. 21(1978)1363–1368.
- [13] C.K. Law, AIAA J. 16(6)(1978)628–630.
- [14] Y.B. Zel'dovich, G.I. Barenblatt, V.B. Librovich, G.M. Makhviladze, The Mathematical Theory of Combustion and Explosions, Consultants Bureau, New York NY, USA, 1985, p.597.
- [15] A.M. Golovin, High Temp. 34(1)(1996)105–111.
- [16] T. Poinsot, D. Veynante, Theoretical and Numerical Combustion, Edwards, Philadelphia PA, USA, 2005, p.538.
- [17] M. D. Smooke, Proc. Comb. Inst. 34(2013)65–98.
- [18] H.G. Weller, G. Tabor, H. Jasak, C. Fureby, J. Comput. Phys. 12(1998)620–631.
- [19] Y. Saad, Iterative Methods for Sparse Linear Systems, SIAM, Philadelphia PA, USA, 2003, p.528.

- [20] E.S. Oran, J.P. Boris, Numerical Simulation of Reactive Flow, Cambridge University Press, New York NY, USA, 2001, p.529.
- [21] I. Demirdzic, Z. Lilek, M. Péric, Int. J. Numer. Meth. Fl. 16(1993)1029–1050.
- [22] R. Mével, S. Javoy, G. Dupré, Proc. Combust. Inst. 33(2011)485–492.
- [23] W. Sutherland, Philos. Mag. Ser. 5. 36(1893)507–531.
- [24] B. Poling, J. Prausnitz, J. O'Connell, The Properties of Gases and Liquids, McGraw Hill Professional, 5th Edition, McGraw-Hill Education, 2000, p.804.
- [25] A. Burcat, R. Branko, Third Millenium Ideal Gas and Condensed Phase Thermochemical Database for Combustion (with Update from Active Thermochemical Tables). Argonne National Laboratory (ANL), July 29, 2005.
- [26] D. Goodwin, Cantera: object-oriented software for reacting flows. Technical Report, California Institute of Technology, 2005.
- [27] J. Melguizo-Gavilanes, L.R. Boeck, R. Mével, J.E. Shepherd, Int. J. Hydrogen Energ. (2016) <http://dx.doi.org/10.1016/j.ijhydene.2016.05.095>
- [28] F.P. Incropera, D.P. DeWitt Fundamentals of Heat and Mass Transfer, Wiley, 4th Edition, 1996, p.912.

## Figure captions

1	Comparison of ignition times obtained from 2-D simulations (unity (solid lines) and non-unity (dashed lines) Le number cases) and CP ignition delay times. . . . .	6
2	Comparison of mass fraction fields ( $H_2$ , $O_2$ , and $N_2$ ) 10 ms after hot sphere contact with reactive mixture with ( $Le \neq 1$ ) and without ( $Le = 1$ ) differential diffusion for $T_{sphere} = 960$ K. . . . .	7
3	Comparison of temperature, velocity and mass fraction fields ( $N_2$ and $H_2O$ ) 16.306 ms after hot sphere contact with reactive mixture with ( $Le \neq 1$ ) and without ( $Le = 1$ ) differential diffusion for $T_{sphere} = 960$ K. . . . .	8
4	wall heat flux along sphere for $T_{sphere} = 960$ K ( $Le = 1$ ). . . . .	8
5	Contributions of each term in the energy equation and temperature normal to the surface of the sphere at $\theta = 120.6^\circ$ for $T_{sphere} = 960$ K ( $Le = 1$ ). . . . .	9
6	Temporal evolution of major and minor species and temperature at ignition location - $\theta = 120.6^\circ$ , 0.081 mm away from surface of the sphere for $T_{sphere} = 960$ K ( $Le = 1$ ). . . . .	10
7	Temporal evolution of $H_2$ , $O_2$ and equivalence ratio, $\Phi$ , for unity (solid lines) and non-unity (dashed lines) Le cases at the ignition location - $\theta = 120.6^\circ$ , 0.081 mm away from surface of the sphere for $T_{sphere} = 960$ K. . . . .	10
8	Temporal evolution of minor species for unity (solid lines) and non-unity (dashed lines) Le number cases at ignition location - $\theta = 120.6^\circ$ , 0.081 mm away from surface of the sphere for $T_{sphere} = 960$ K. . . . .	11